Inorganic Chemistry

Article

pubs.acs.org/IC

Analysis of the Putative Cr−Cr Quintuple Bond in Ar′CrCrAr′ (Ar′ = C_6H_3-2,6(C_6H_3-2,6-Pr^i_2)$_2$ Based on the Combined Natural Orbitals for Chemical Valence and Extended Transition State Method

Sylvester Ndambuki and Tom Ziegler*

Department of Chemistry, University of Calgary, Calgary, Alberta, Canada T2N1N4

Supporting Information

ABSTRACT: The nature of the putative Cr−Cr quintuple bond in Ar′CrCrAr′ (Ar′ = C_6H_3-2,6(C_6H_3-2,6-Pr^i_2)$_2$) is investigated with the help of a newly developed energy and density decomposition scheme. The new approach combines the extended transition state (ETS) energy decomposition method with the natural orbitals for chemical valence (NOCV) density decomposition scheme within the same theoretical framework. The results show that in addition to the five bonding components ($\sigma^2\pi^2\pi'^2\delta^2\delta'^2$) of the Cr−Cr bond, the quintuple bond is augmented by secondary Cr−C interactions involving the Cr-*ipso*-carbon of the flanking aryl rings. The presence of isopropyl groups (Pr^i) is further shown to stabilize Ar′CrCrAr′ by 20 kcal/mol compared to the two Ar′Cr monomers through stabilizing van der Waals dispersion interactions.

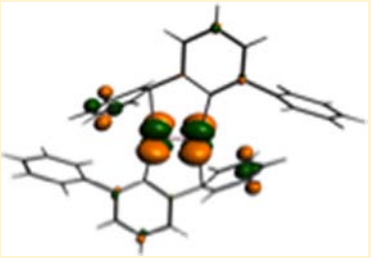

I. INTRODUCTION

The recently[1] synthesized dichromium complex Ar′CrCrAr′ (Ar′ = C_6H_3-2,6(C_6H_3-2,6-Pr^i_2)$_2$) with a C_{2h} geometry has stimulated several[2−8] theoretical and experimental studies in which the nature of the Cr−Cr bond was probed. It has been asserted that the unusually short Cr−Cr distance (1.835 Å) is indicative of a quintuple bond ($\sigma^2\pi^4\delta^4$). The complex has in addition a Cr−Cr−C angle of 101° which allows for a secondary Cr−C interaction between one chromium center and an *ipso*-carbon of one of the flanking aryl rings attached to the other chromium center. This interaction has been alleged further to stabilize the Cr−Cr link. The fact that RCrCrR complexes only have been isolated with bulky R groups also indicates that ligands such as Ar′ serve to provide steric protection. However, it has moreover been suggested that the electron donating isopropyl substituents (Pr^i) on the aryl rings might help stabilize the metal bond electronically. After the initial work by Power[1] et al., several complexes with ultrashort Cr−Cr bonds have been reported.[3−5] The shortest Cr−Cr distance (1.7293 Å) to date has been observed by Kempe[6] et al.

It is the objective of the present study to probe the strength and multiplicity of the Cr−Cr bond in Ar′CrCrAr′ as well as the *ipso*-carbon−chromium interaction by the help of the extended transition state (ETS) energy decomposition scheme[9] and the natural orbitals for chemical valence (NOCV) density decomposition approach.[10−14] These techniques have recently been combined into the ETS-NOCV method.[11] We shall further assess whether Ar′ is able electronically to stabilize the Cr−Cr bond either by electron donation from the isopropyl substituents (Pr^i) on the aryl rings or through dispersive van der Waals attractions between the two Ar′ ligands.

II. COMPUTATIONAL METHODS AND DETAILS

We provide here a brief account of the ETS-NOCV method.

Extended Transition State Method (ETS). The ETS scheme considers the formation of a molecule AB with the corresponding ground state Kohn−Sham wave function Ψ_{AB} and energy E_{AB} to be formed from two (or more) non-interacting fragments A^0 and B^0 with energies E^0_A and E^0_B, respectively. In the first instance, the two interacting fragments are distorted at infinite separation from their equilibrium geometries to the structures A and B they will have in the combined molecule AB. The energy that is required for this distortion is given as

$$\Delta E_{prep} = E_A - E^0_A + E_B - E^0_B \quad (1)$$

where E_A and E_B are the energies of the distorted fragments A and B, respectively. The ETS scheme decomposes the difference ΔE_{int} between the energy of the combined molecule E_{AB} and the energies of the distorted fragments E_A and E_B into various chemically meaningful components as

$$\Delta E_{int} = \Delta E_{elst} + \Delta E_{Pauli} + \Delta E_{disp} + \Delta E_{orb} \quad (2)$$

Here ΔE_{elst} is the electrostatic interaction[9] between the two distorted fragments as they are brought from infinite separation to their final positions in the combined molecule without any change in density. This term is stabilizing for neutral fragments. Further, ΔE_{Pauli} represents the destabilizing[9] interaction between the occupied orbitals on A and B, respectively. This destabilization is also referred to as the Pauli repulsion.[9] It is customary[9,16] to combine ΔE_{elst} and ΔE_{Pauli} into the steric interaction energy $\Delta E_{steric} = \Delta E_{elst} + \Delta E_{Pauli}$. Further, ΔE_{disp} is the stabilizing van der Waals dispersion interactions[17] between the two fragments A and B in AB. Allowing finally the virtual orbitals on A and B to participate in the bonding leads to the orbital stabilization term $\Delta E_{orb}$of eq 2. Participation of the virtual orbitals gives rise to the change in density[9]

Received: April 21, 2012
Published: June 25, 2012

   dx.doi.org/10.1021/ic300824u | *Inorg. Chem.* 2012, 51, 7794−7800

$$\Delta\rho = \sum_{\lambda}\sum_{\mu} \Delta P_{\mu\lambda}\psi_{\lambda}(1)\psi_{\mu}(1) \quad (3)$$

Here the summation over (μ,λ) involves both occupied and virtual orbitals (ψ_μ,ψ_λ) of the two deformed fragments and $\Delta P_{\mu\lambda}$ is the density matrix that spans $\Delta\rho$ in the orbital space (ψ_μ,ψ_λ). In fact the set (ψ_μ,ψ_λ) used in eq 3 consists of orthogonalized fragment orbitals[11] constructed from the original nonorthogonal set[11] $(\psi'_\mu,\psi'_\lambda)$ by Schmidt orthogonalizing virtual orbitals on occupied orbitals[11] and each other. Further, the occupied orbitals are Lowdin orthogonalized.[11] The two sets (ψ_μ,ψ_λ) or $(\psi'_\mu,\psi'_\lambda)$ are equivalent in that both can be used to represent ΔE_{orb} or $\Delta\rho$. However, (ψ_μ,ψ_λ) has some desirable properties that we shall mention shortly.

The density change $\Delta\rho$ is often referred to as the bond deformation density and $\Delta P_{\mu\lambda}$ is named the bond deformation density matrix. We can write[9,12,13] the deformation energy as

$$\Delta E_{orb} = \sum_{\lambda}\sum_{\mu} \Delta P_{\lambda\mu} F^{TS}_{\lambda\mu} \quad (4)$$

Here $F^{TS}_{\lambda\mu}$ is a Kohn−Sham Fock matrix element that is defined in terms of a transition state potential at the midpoint between the combined fragments and the final molecule, hence the word extended transition state (ETS) method.[9,11,12] For symmetrical molecules ΔE_{orb} can be split into contributions from the different irreducible representations[12,13] Γ_i of the molecule point group Γ_i as

$$\Delta E_{orb} = \sum_{i}^{rep} \Delta E^{\Gamma_i} \quad (5)$$

In favorable cases different interactions such as σ,π,δ-bonding or σ-donation and π-back-donation can be attributed to different representations and thus assessed individually.[12,13] Unfortunately, for many molecules with low or no symmetry such a separation is not possible with ETS.

Natural Orbitals for Chemical Valence (NOCV). In the NOCV approach[10] ΔP is diagonalized. Thus

$$C_i^{+}\Delta P C_i = v_i; \quad i = 1, M \quad (6)$$

where M denotes the total number of fragment orbitals and C_i is a column vector containing the eigenvectors to ΔP. We next introduce the NOCVs as

$$\varphi_i(1) = \sum_{\lambda}^{M} C_{i\lambda}\psi_{\lambda}(1) \quad (7)$$

It is obvious from eqs 6 and 7 that we can write $\Delta\rho$ as

$$\Delta\rho = \sum_{i}^{N} v_i\varphi_i(1)\varphi_i(1) \quad (8)$$

In the particular case where we are using orthogonalized fragment orbitals in eq 7 we get[11] pairs of eigenvalues (v_i,v_j) that are equal in absolute terms but of opposite signs. We can thus in that case write

$$\Delta\rho(1) = \sum_{k=1}^{M/2} v_k[-\varphi^2_{-k}(1) + \varphi^2_k(1)] = \sum_{k=1}^{M/2} \Delta\rho_k(1) \quad (9)$$

where the deformation density $\Delta\rho$ is expressed in the NOCV representation as a sum of pairs of complementary eigenfunctions (ϕ_k,ϕ_{-k}) corresponding to the eigenvalues v_k and v_{-k} with the same absolute value but opposite signs. Historically the use of NOCVs goes back to the Nalewajski−Mrozek valence theory.[14,15]

ETS-NOCV Scheme. Expressing ΔE_{orb} of eq 4 in terms of the NOCVs leads to the simple expression

$$\Delta E_{orb} = \sum_{k=1}^{M/2} v_k[-F^{TS}_{-k,-k} + F^{TS}_{k,k}] \quad (10)$$

where $F^{TS}_{-k,-k}$ and $F^{TS}_{k,k}$ are diagonal Kohn−Sham matrix elements defined over NOCVs with respect to the transition state (TS) intermediate between the density of the final molecule AB and the superimposed fragment densities of A and B.[9] In deriving eq 10 use has been made of the fact that the coefficients C_i that define the NOCVs are eigenvectors to ΔP. The advantage of the expression in eq 10 for ΔE_{orb} over that of eq 4 is that only a few complementary NOCV pairs normally contribute significantly to ΔE_{orb}. It can further be seen from eqs 9 and 10 that, for each complementary NOCV pair representing one of the charge deformations $\Delta\rho_k$ we have as well the corresponding bond energy contribution ΔE^{orb}_k.[11] Also, the individual contributions $\Delta\rho_k$ can usually be interpreted in terms of interactions such as σ,π,δ-bonding or σ-donation and π-back-donation even when the molecule AB lacks symmetry.

Computational Details. All DFT calculations presented here were based on the Amsterdam density functional program version 2010.01 in which the ETS-NOCV was implemented.[18] Use was made of the Becke−Perdew exchange-correlation functional (BP86)[19,20] and a standard triple-ζ STO basis with one set of polarization functions for all atoms. Relativistic effects for Cr atom were included at the scalar relativistic ZORA level of approximations as implemented in the ADF program.[18] The fragment and molecular orbitals, as well as contours of deformation densities were plotted using the ADF-GUI interface.[18] The calculations on Ar′CrCrAr′ (Ar′ = C_6H_3-2,6(C_6H_3-2,6-Pr^i_2)$_2$) were based on the published[1] crystal structure. The positions of the hydrogen atoms were optimized while keeping all other atoms at frozen positions. The Cartesian coordinates for Ar′ = C_6H_3-2,6(C_6H_3-2,6-Pr^i_2)$_2$ and the model system Ar* = C_6H_3-2,6(C_6H_5)$_2$ are given in the Supporting Information, Tables S1 and S2, respectively. The dispersion term ΔE_{disp} of eq 2 was taken from the dispersion corrected DFT scheme by Grimme et al.[17] as implemented in ADF.

III. RESULTS AND DISCUSSION

Electronic Structure of Ar*CrCrAr*. The molecular orbitals of Ar′CrCrAr′ (Ar′ = C_6H_3-2,6(C_6H_3-2,6-Pr^i_2)$_2$) (**1**) and the model system Ar*CrCrAr* (Ar* = C_6H_3-2,6(C_6H_5)$_2$) (**2**) where the Pr^i groups have been replaced by hydrogens are well-known and firmly established by previous studies.[1−8] Nevertheless, we present for the sake of completeness the five metal−metal bonding orbitals along with the constituent fragment orbitals for the model system **2** in Figure 1. At lowest energy are the two π-type components $1a_u$ (π^x) and $1b_u$ (π^y)of Figure 1. They are in-phase combinations of respectively the d_{xy} and d_{yz} fragment orbitals in a local right-handed coordinate system where the z-axis is pointing along the Cr−C bond and the x-axis is perpendicular to the C−Cr−Cr plane, Figure 1. Higher in energy is $1a_g$ (σ) as a bonding combination of two mostly $d_{x^2-y^2}$ fragment orbitals. At highest energy are $2a_g$ (δ') and $1b_g$ (δ). Here $1b_g$ (δ) can unambiguously be characterized as δ-bonding since it is made up of two d_{xz} orbitals. On the other hand, $2a_g$ (δ') is an in-phase combination of two δ' fragment orbitals where each δ' has 49.39% 4s-character, 25.12% d_{z^2}, 13.42% d_{xy} and 10.2% $d_{x^2-y^2}$, see left panel of Figure 1b. With 100% d_{z^2} the $2a_g$ (δ') component would be δ-bonding. However, in agreement with ligand field theory d_{z^2} is mostly part of a C−Cr antibonding orbital of higher energy. Instead δ' is a metal hybrid dominated by 4s with some participation from d_{z^2}. Thus $2a_g$ (δ') is better referred to as a (δ/σ) bonding orbital made up of two in-phase δ' components that each are 2-fold symmetric with respect to rotations around the CCr and CrCr bond without changing sign. The same shape for $2a_g$ (δ') can also be seen in previously published contours of this orbital.[1]

NOCV-ETS Analysis of the Cr−Cr Bond in Ar*CrCrAr* and Ar′CrCrAr′. Table 1 (top) affords the ETS analysis of a Cr−Cr bond formed from two Ar*Cr fragments with a hextet ground state valence configuration ($\sigma^1\pi^1\pi^1\delta'^1\delta^1$) and opposite spin polarization (Ar*Cr ↑↑↑↑↑ and ↓↓↓↓↓CrAr*). The two

dx.doi.org/10.1021/ic300824u | Inorg. Chem. 2012, 51, 7794−7800

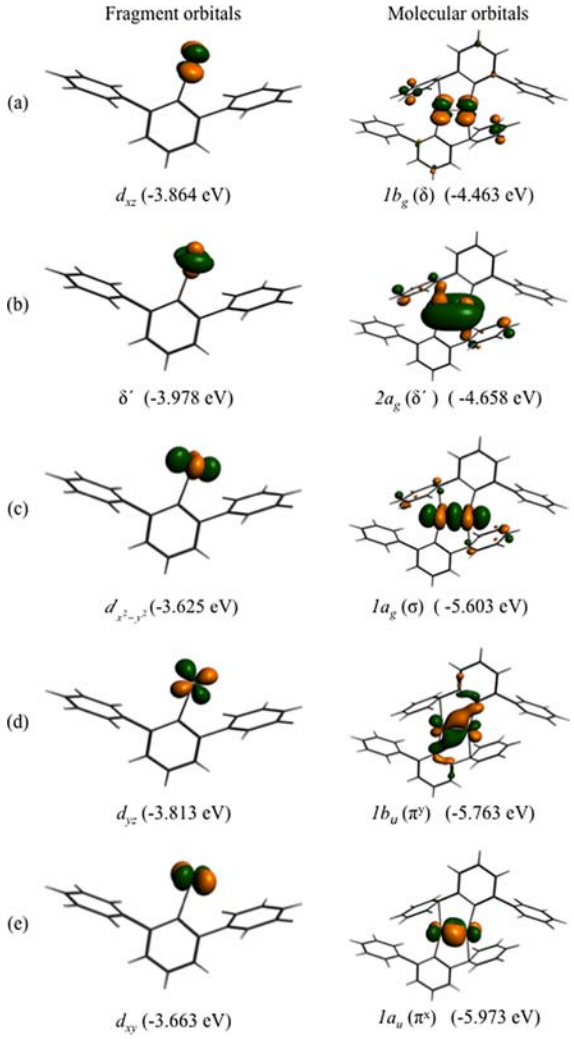

Figure 1. Metal fragment and molecular orbitals with their corresponding energies for the Cr−Cr bonding orbitals in Ar*CrCrAr*.

fragments are already considered to have the geometry of the final combined complex. Thus, no attempt is made to determine the preparation energy ΔE_{prep} of eq 1 as we are primarily interested in the relative strength of the various Cr−Cr bonding modes. It follows from Table 1(top) that the total steric interaction energy $\Delta E_{steric} = \Delta E_{elst} + \Delta E_{Pauli}$ between the two fragments amounts to 175.52 kcal/mol. It is composed of the stabilizing electrostatic term ΔE_{elst} of −401.06 kcal/mol and the Pauli repulsion contribution with a value of 576.58 kcal/mol. The total Cr−Cr bond formation energy $\Delta E_{int} = \Delta E_{orb} + \Delta E_{steric} + \Delta E_{disp}$ is negative (stabilizing) with ΔE_{int} = −91.04 kcal/mol thanks to the orbital interaction energy ΔE_{orb} of −248.32 kcal/mol and the stabilizing van der Waals dispersion interactions[17] between the two ArCr* fragments given by ΔE_{disp}= −18.24 kcal/mol.

Table 2 (top) presents a NOCV decomposition of ΔE_{orb} according to

$$\Delta E_{orb} = \Delta E_{orb}^{\pi^y} + \Delta E_{orb}^{\pi^x} + \Delta E_{orb}^{\sigma} + \Delta E_{orb}^{\delta} + \Delta E_{orb}^{\delta'} + \Delta E_{orb}^{sec} + \Delta E_{orb}^{sec'} + \Delta E_{orb}^{pol} \quad (11)$$

Here $\Delta E_{orb}^{\pi^y}$ is the contribution from the π^y-bond in the CCrCrC symmetry plane of **2** whereas $\Delta E_{orb}^{\pi^x}$ is the corresponding contribution from the π^x-bond perpendicular to the symmetry plane. The π^y-bond is seen to be formed by a flow of α-electron density ($\Delta\rho_{orb}^{\pi^y,\alpha}$) from a d_{yz} orbital on the right-hand center (yellow) to a d_{yz} orbital on the left-hand side (Green), (c) of Figure 2. At the same time β-electron density ($\Delta\rho_{orb}^{\pi^y,\beta}$) is flowing between d_{xy} electrons in the opposite direction. For the π^x-bond perpendicular to the symmetry plane the flow of density is between d_{xz} orbitals, (b) of Figure 2. In absolute terms the π^y-bond with $\Delta E_{orb}^{\pi^y}$ = −71.84 kcal/mol is somewhat more stabilizing than the π^x-bond with $\Delta E_{orb}^{\pi^x}$ = −49.78 kcal/mol, a point that will be discussed further shortly. We have further in Figure 2 as (a) the σ-bond formation involving primarily $d_{x^2-y^2}$ orbitals. The σ-link is marginally weaker than the π^x-bond with ΔE_{orb}^{σ} = −45.22 kcal/mol. We finally have the two δ-type bonds $\Delta\rho_{orb}^{\delta'}$ and $\Delta\rho_{orb}^{\delta}$ in Figure 3. Here the δ'-bond involving the two δ' metal hybrids is the strongest with $\Delta E_{orb}^{\delta'}$ −32.10 kcal/mol, Figure 3b. However, the strength of this bond is visibly aided by some Cr−C_{ipso} interaction. The other δ-bond $\Delta\rho_{orb}^{\delta}$ due to the two d_{xz} orbitals is considerably weaker with ΔE_{orb}^{δ} = −13.10 kcal/mol, Figure 3a.

There has been considerable interest in the role played by the Cr−C_{ipso} interaction in stabilizing the bond between the two Ar*Cr fragments.[1,25] We have already noticed some participation of this interaction in $\Delta\rho_{orb}^{\delta'}$. However, the major contributions from the Cr−C_{ipso} interaction can be seen in Figure 4 as $\Delta\rho_{orb}^{sec}$ and $\Delta\rho_{orb}^{sec'}$. They represent flow of charge from the central aryl-rings as well as the metal centers to the Cr−C_{ipso} bonding region. The combined stabilization amounts to $\Delta E_{orb}^{sec} + \Delta E_{orb}^{sec'}$ = −23.06 kcal/mol. We finally have the remainder $\Delta\rho_{orb}^{rest}$ of $\Delta\rho_{orb}$ not accounted for so far. It seems also to represent accumulation of charge in the Cr−C_{ipso} bonding region. Adding ΔE_{orb}^{rest} = −15.11 kcal/mol to $\Delta E_{orb}^{sec} + \Delta E_{orb}^{sec'}$ leads to a combined stabilization for the Cr−C_{ipso} bond of −38.17 kcal/mol. Thus the Cr−C_{ipso} interaction is stronger than the δ-bond but somewhat weaker than the σ, π, and δ' bonds.

Turning next to the complete Ar′CrCrAr′ system **1** we find from Table 1 that $\Delta E_{steric} = \Delta E_{elst} + \Delta E_{Pauli}$ as expected has increased slightly from 175.52 kcal/mol in **2** to 179.30 kcal/mol in **1**. The five M-M bonding components $\Delta E_{orb}^{\pi^y} + \Delta E_{orb}^{\pi^x} + \Delta E_{orb}^{\sigma} + \Delta E_{orb}^{\delta} + \Delta E_{orb}^{\delta'}$ have combined and gone from −212.04 kcal/mol (**2**) to −212.98 kcal/mol (**1**) with deviations in the individual contributions of 2−3 kcal/mol. Thus the Pr^i

Table 1. ETS Analysis[c] for Ar*CrCrAr* and Ar′CrCrAr′

compound	E_{elst}	ΔE_{Pauli}	ΔE_{steric}[b]	ΔE_{orb}	ΔE_{disp}	ΔE_{int}[a]
Ar*CrCrAr*[d]	−401.06	576.58	175.52	−248.32	−18.24	−91.04
Ar′CrCrAr′[e]	−421.09	600.40	179.30	−256.26	−39.49	−116.44

[a]Total bonding energy: $\Delta E_{int} = \Delta E_{steric} + \Delta E_{orb} + \Delta E_{disp}$. [b]Steric interaction: $\Delta E_{steric} = \Delta E_{Pauli} + \Delta E_{elstat}$. [c]Energies in kcal/mol. [d](Ar* = C_6H_3-2,6(C_6H_5)$_2$). [e](Ar′ = C_6H_3-2,6(C_6H_3-2,6-Pr$^i_2$)$_2$).

dx.doi.org/10.1021/ic300824u | Inorg. Chem. 2012, 51, 7794−7800

Table 2. NOCV Contributions[a,b] to[a] ΔE_{orb} in Ar*CrCrAr* and Ar′CrCrAr′

compound	$\Delta E^{\pi'}_{orb}$	$\Delta E^{\pi^*}_{orb}$	ΔE^{σ}_{orb}	$\Delta E^{\delta'}_{orb}$	ΔE^{δ}_{orb}	ΔE^{sec}_{orb}	$\Delta E^{sec'}_{orb}$	ΔE^{rest}_{orb}	ΔE_{orb}
Ar*CrCrAr*	−71.84	−49.78	−45.22	−32.10	−13.10	−13.41	−9.65	−15.11	−248.32
Ar′CrCrAr′	−72.73	−49.44	−41.61	−32.61	−16.89	−13.79	−9.23	−21.79	−256.26

[a] $\Delta E_{orb} = \Delta E^{\pi'}_{orb} + \Delta E^{\pi^*}_{orb} + \Delta E^{\sigma}_{orb} + \Delta E^{\delta}_{orb} + \Delta E^{\delta'}_{orb} + \Delta E^{sec}_{orb} + \Delta E^{sec'}_{orb} + \Delta E^{rest}_{orb}$ [b] Energies in kcal/mol.

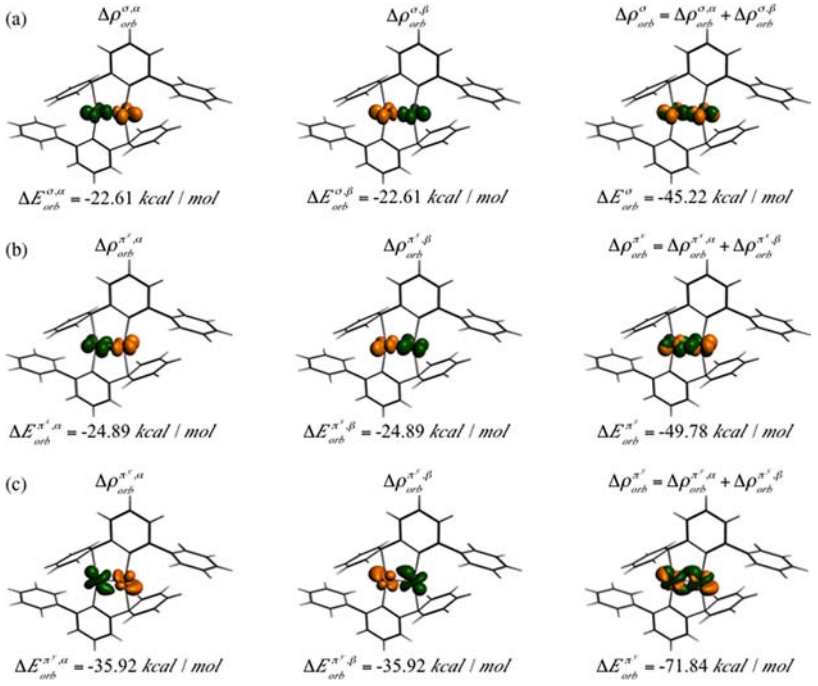

Figure 2. Contours of the NOCV deformation densities representing π- and σ-bonding. The contour values are +0.03 au. Green represents positive and orange negative.

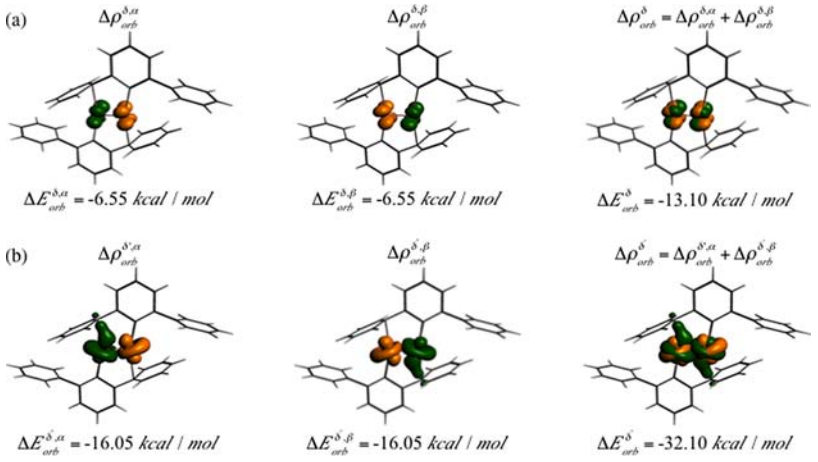

Figure 3. Contours of the NOCV deformation densities representing δ'- and δ-bonding. The contour values are +0.03 au. Green represents positive and orange negative.

substituents seem hardly to influence the M-M bonding interactions. The sum of the two secondary interactions ΔE^{sec}_{orb} $\Delta E^{sec'}_{orb}$ is also insensitive to adding Pr^i . On the other hand the ΔE^{rest}_{orb} becomes more stabilizing by −6.68 kcal/mol as we introduce Pr^i. When ΔE_{steric} and ΔE_{orb} are combined the two fragments are 4.16 kcal/mol more strongly bound together in **1** compared to **2**. However, the remaining term ΔE_{disp} due to the dispersive van der Waals attractions is seen to be much more stabilizing for the real system **1** where ΔE_{disp} = −39.49 kcal/mol than for the model system **2** where ΔE_{disp} = −18.24 kcal/mol, Table 1. Thus, introducing the Pr^i substituents is seen to stabilize the monomer primarily through ΔE_{disp}.

Dependence of Dispersion and the Orbital Interaction Components on the trans-Bending Angle. We illustrate in Table 3 the dependence of dispersion ΔE_{disp} and the intrinsic bonding components (ΔE_{elst}, ΔE_{pauli}, ΔE_{orb}) on the trans-bending angle $\Phi = 180° - \angle CCrCr$ in Ar*CrCrAr*, where for ΔE_{disp}, use is made of the expression and parametrization by Grimme.[23] During the variation of Φ both the Cr−Cr distance and the structure of Ar* were kept frozen.

dx.doi.org/10.1021/ic300824u | Inorg. Chem. 2012, 51, 7794−7800

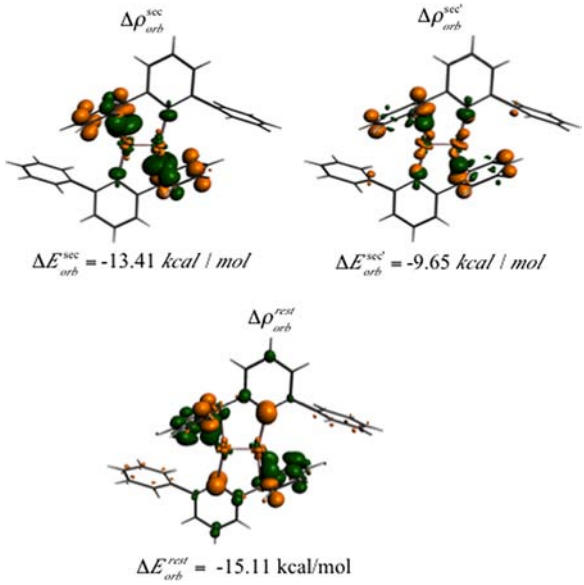

Figure 4. Contours of the NOCV deformation densities for the Cr−C_{ipso} secondary interactions and the remainder with the corresponding orbital interaction energies. The contour values are 0.03 a.u for secondary interactions and 0.003 a.u for the remainder . Green represents positive and orange negative.

Table 3. ETS Analysis[c,d] for Ar*CrCrAr* Using BP86 at Different Cr−Cr−C Angles

Φ^e	ΔE_{elst}	ΔE_{Pauli}	$\Delta E_{steric}{}^b$	ΔE_{orb}	ΔE_{disp}	$\Delta E_{int}{}^a$
0	−13.71	124.03	110.32	−118.42	−7.80	−15.90
35	−117.81	245.03	127.23	−127.69	−16.48	−16.95
40	−142.28	270.81	128.53	−132.31	−17.57	−21.34
50	−312.41	501.27	188.87	−236.64	−18.83	−66.60
60	−382.16	579.01	196.85	−259.48	−19.44	−82.07
70	−415.58	609.63	194.05	−265.42	−19.55	−90.93
79	−401.06	576.58	175.52	−248.32	−18.24	−91.04
90	−386.68	556.62	169.94	−237.42	−19.35	−86.83

[a]Total bonding energy: $\Delta E_{int} = \Delta E_{steric} + \Delta E_{orb} + \Delta E_{disp}$. [b]Steric interaction: $\Delta E_{steric} = \Delta E_{Pauli} + \Delta E_{elstat}$. [c]Energies in kcal/mol. [d](Ar* = C_6H_3-2,6(C_6H_5)$_2$). [e]Trans bending angle Φ = 180° − ∠CCrCr in degrees.

We recall in addition that the structure of Ar*CrCrAr* has been obtained from Ar′CrCrAr′ by replacing the Pr^i groups by hydrogens.

It follows from Table 3 that both the orbital energy ΔE_{orb} and the dispersion ΔE_{disp} term have minima at 70°. However, the steric interaction energy ΔE_{steric} has a maximum at 60° and decreases for larger Φ. As a consequence, the minimum for the combined interaction energy $\Delta E_{int} = \Delta E_{steric} + \Delta E_{orb} + \Delta E_{disp}$ is shifted closer to the observed trans-bending angle of 79° for Ar′CrCrAr′.

In Table 4 we display the different components of the orbital interaction energy ΔE_{orb} as a function of Φ. The corresponding deformation densities are shown in Figures 2−4 for Φ = 79° and in Supporting Information, Figures S1−S2 for Φ= 0°. We notice first of all that the secondary interactions $\Delta\rho^{sec}_{orb}$ and $\Delta\rho^{sec'}_{orb}$ are absent as individual NOCV contributions for 0° ≤ Φ ≤ 40°. For Φ > 40° ΔE^{sec}_{orb}, $\Delta\rho^{sec'}_{orb}$ emerges as individual stabilizing NOCV components with a minimum for ΔE^{sec}_{orb} + $\Delta E^{sec'}_{orb}$ around 79°.

There are two symmetry orbitals contributing to the "δ-bonding" component ΔE^{δ}_{orb}, namely, $1b_g$ (Φ) and $2b_g$ (Φ) of Figure 5a. The term ΔE^{δ}_{orb} is positive at Φ = 0° where the δ-bond is represented solely by $2b_g$ (Φ = 90°), Supporting Information, Figure S2a. It goes through a minimum at Φ = 70° where $1b_g$ (Φ = 70°) is seen to be δ-bonding. However the π^* combination $2b_g$ (Φ = 70°) has a positive overlap with $1b_g$ (Φ = 70°) and can thus contribute in a stabilizing fashion to $1b_g$ (δ) of Figure 1a. At the minimum ΔE^{δ}_{orb} is stabilizing with ΔE^{δ}_{orb} −17.49 kcal/mol.

The other δ'-component has contributions from the three symmetry orbitals (na_g (Φ); n = 1,3) of Figure 5. The corresponding energy $\Delta E^{\delta'}_{orb}$ starts out positive at Φ = 0° where the δ'-component is represented solely by $2a_g$ (Φ = 0°), Supporting Information, Figure S2b. It decreases throughout the interval 0° < Φ < 90° and becomes negative at Φ = 40°, Table 4. The decrease is due to the contribution from the Cr−C_{ipso} interaction as it can be seen at the equilibrium structure with Φ = 79° in the plot of the δ'-bonding molecular orbital $1b_g$ (δ), Figure 1b, as well as the plot of $\Delta E^{\delta'}_{orb}$, Figure 2c. In both cases the dominating symmetry orbital is $3a_g$ (Φ). In the interval 0° ≤ Φ ≤ 40° where both $\Delta E^{\delta'}_{orb}$ and ΔE^{δ}_{orb} are positive the system would prefer a $(\delta')^1(\delta)^1(\delta'^*)^1(\delta^*)^1$ high-spin configuration rather than the low spin $(\delta')^2(\delta)^2$ configuration.

The σ-bond has as the δ'-component contributions from the three symmetry orbitals (na_g (Φ); n = 1,3). At Φ = 0° ΔE^{σ}_{orb} is represented by $3a_g$ (Φ = 0°), Supporting Information, Figure S1a and Figure 5e. Here $3a_g$ (Φ = 0°) is an in-phase linear combination of the two δ' fragment orbitals, Figure 1b. As Φ increases $1a_g$ (Φ) and $2a_g$ (Φ) becomes dominant and ΔE^{σ}_{orb} reaches a minimum at Φ = 50° with ΔE^{σ}_{orb} = −57.61 kcal/mol where $1a_g$ (Φ) has reached its maximal bonding overlap whereas that of $2a_g$ (Φ) still is growing. At the equilibrium structure ΔE^{σ}_{orb} is dominated by $2a_g$ (Φ = 79°) with some contribution from $1a_g$ (Φ = 79°), Figures 2a, and ΔE^{σ}_{orb} has risen to −45.22 kcal/mol.

Table 4. NOCV Contributions[a,b] to $\Delta E_{orb}{}^a$ in Ar*CrCrAr* Using BP86 at Different Angles

Cr−Cr−C	$\Delta E^{\pi'}_{orb}$	$\Delta E^{\pi^*}_{orb}$	ΔE^{σ}_{orb}	ΔE^{δ}_{orb}	$\Delta E^{\delta'}_{orb}$	ΔE^{sec}_{orb}	$\Delta E^{sec'}_{orb}$	ΔE^{rest}_{orb}	ΔE_{orb}
0	−50.02	−44.49	−35.41	12.28	11.88	−9.45	−118.42		
35	−44.70	−41.16	−26.13	2.86	9.78	−7.76	−127.69		
40	−43.65	−42.09	−39.65	3.63	−0.69	−9.22	−132.31		
50	−60.83	−53.47	−57.69	−9.00	−18.18	−13.10	−10.79	−14.52	−236.64
60	−72.69	−53.39	−55.57	−15.10	−23.42	−14.01	−11.05	−15.93	−259.48
70	−78.88	−52.36	−47.18	−17.49	−30.25	−14.66	−11.99	−14.71	−265.42
79	−71.84	−49.78	−45.22	−13.10	−32.10	−13.41	−9.65	−15.11	−248.32
90	−67.31	−48.90	−38.33	−8.00	−36.14	−15.30	−9.91	−15.44	−237.42

[a]$\Delta E_{orb} = \Delta E^{\pi'}_{orb} + \Delta E^{\pi^*}_{orb} + \Delta E^{\sigma}_{orb} + \Delta E^{\delta}_{orb} + \Delta E^{\delta'}_{orb} + \Delta E^{sec}_{orb} + \Delta E^{sec'}_{orb} + \Delta E^{rest}_{orb}$. [b]Energies in kcal/mol.

dx.doi.org/10.1021/ic300824u | Inorg. Chem. 2012, 51, 7794−7800

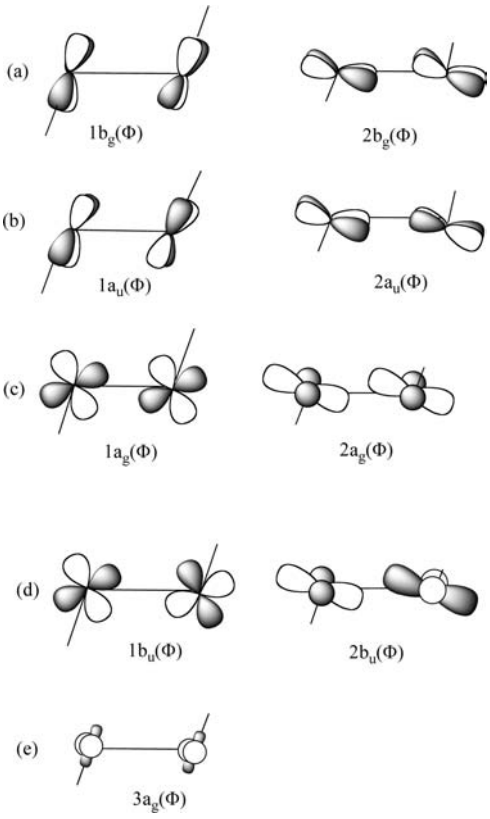

Figure 5. Symmetry orbitals participating in the σ, π, and δ bonding drawn at the equilibrium structure with $\Phi = 79°$. The same symmetry combinations are obtained for other trans bending angles Φ by rotating the fragment orbitals on the two centers rigidly and synchronously with the C−Cr bonds.

It follows from Table 4 that the π^y-bond in the CCrCrC plane has the most stabilizing orbital contribution $\Delta E^{\pi^y}_{orb}$. At $\Phi = 0°$ it starts out as a regular π-bond described solely by 1b$_u$ ($\Phi = 0°$), see Supporting Information, Figure S1b and Figure 5d. As Φ increases $\Delta E^{\pi^y}_{orb}$ reaches a minimum at $\Phi = 70°$ with $\Delta E^{\pi^y}_{orb} = -78.88$ kcal/mol. At the nearby equilibrium structure with $\Phi = 79°$we find $\Delta E^{\pi^y}_{orb} = -71.84$ kcal/mol. In both cases the bond is described by the π-orbital 1b$_u$ (Φ) augmented by the σ*-orbital 2b$_u$ (Φ) through the large overlap between the two symmetry combinations, Figures 1d and 2c.

We finally have the out-of-plane π^x-bond that has a rather steady $\Delta E^{\pi^y}_{orb}$ which is maintained throughout the Φ range by 1a$_u$ (Φ) and 2a$_u$ (Φ), Figure 5b. At $\Phi = 0°$ the symmetry orbital 1a$_u$ ($\Phi = 0°$) makes up the π^x-bond and $\Delta E^{\pi^y}_{orb} = -44.49$ kcal/mol, Supporting Information, Figure S1c. The term $\Delta E^{\pi^x}_{orb}$ has a shallow minimum at $\Phi = 50°$ with $\Delta E^{\pi^x}_{orb} = -53.47$ kcal/mol and attain a value of $\Delta E^{\pi^x}_{orb} = -49.78$ kcal/mol at the equilibrium structure where the π^x-bonding mostly is due to 2a$_u$ ($\Phi = 79°$), Figures 1e and 2b . A more general discussion of quintuple bonds have been given elsewhere.[1−8,21−24]

IV. CONCLUDING REMARKS

We have applied the NOCV-ETS decomposition scheme to a study of the putative Cr−Cr quintuple bond in Ar′CrCrAr′ (Ar′ = C$_6$H$_3$-2,6(C$_6$H$_3$-2,6-Pr$^i_2$)$_2$) **1**. This complex has a trans-bent structure with a Cr−Cr−C angle of 101° and a short Cr−Cr bond length of 1.835 Å. It follows from the NOCV-ETS analysis that the trans bending is favorable since it leads to a stabilization of the σ, π, and δ bonding component. Our ETS-NOCV calculations indicate that the two δ-components are weak in the linear conformation where the Cr−Cr−C angle is 180°. In that case **1** would adopt a $(\delta')^1(\delta)^1(\delta'^*)^1(\delta^*)^1$ high-spin configuration rather than a low spin $(\delta')^2(\delta)^2$ configuration. Thus, the linear geometry **1** only retains a triple bond, Table 4. However in the trans bent geometry both δ-components are stabilized adopting a low spin $(\delta')^2(\delta)^2$ configuration. Thus, trans bent **1** clearly can be characterized as having a quintuple bond, Table 4. The trans bent structure is further favored by a Cr−C$_{ipso}$ interaction that contributes with $\Delta E^{\delta'}_{orb} + \Delta E^{\delta}_{orb} = -23$ kcal/mol to its stability relative to the linear conformation.

We have also been able to address the role of the Pr^i-substituents in **1** by comparing to calculations on the model system Ar*CrCrAr* (Ar* = C$_6$H$_3$-2,6(C$_6$H$_5$)$_2$) **2** where the Pr^i groups have been replaced by hydrogens. Our NOCV-ETS analysis indicates that the electron donating abilities of the Pr^i groups only have a marginal influence on the quintuple bond. On the other hand, the Pr^i-substituents add considerably extra stability (20 kcal/mol) to the Ar′CrCrAr′ dimer compared to the two Ar′Cr monomers by adding stabilizing dispersive van der Waals attractions between the two Ar′ ligands. The addition of even more isopropyl substituents to Ar has been observed experimentally[25] eventually to destabilize CrAr compared to ArCrCrAr as any net gain from further dispersion stabilization is balanced out by increasing steric destabilization. We have finally shown that the optimal trans bending angle differs among the various σ, π, and δ bonding component. This is the first study that is able to quantify the different bonding contributions and delineate their relative importance as a function of the trans bending angle.

■ ASSOCIATED CONTENT

Ⓢ Supporting Information

Figure S1, contours of the NOCV deformation densities representing π- and σ-bonding at $\Phi = 0°$. Figure S2, contours of the NOCV deformation densities representing δ'- and δ-bonding at $\Phi = 0°$. The Cartesian coordinates for Ar′ = C$_6$H$_3$-2,6(C$_6$H$_3$-2,6-Pr$^i_2$)$_2$ and the model system Ar* = C$_6$H$_3$-2,6(C$_6$H$_5$)$_2$ are given in Tables S1 and S2, respectively. This material is available free of charge via the Internet at http://pubs.acs.org.

■ AUTHOR INFORMATION

Corresponding Author

*E-mail: ziegler@ucalgary.ca.

Notes

The authors declare no competing financial interest.

■ ACKNOWLEDGMENTS

We are grateful to WESTGRID for access to computational facilities. T.Z thanks the Canadian Government for a Canada Research Chair.

■ REFERENCES

(1) Nguyen, T.; Sutton, A. D.; Brynda, M.; Fettinger, J. C.; Long, G. J.; Power, P. P. *Science* **2005**, *310*, 844.

(2) Brynda, M.; Gagliardi, L.; Roos, B. O. *Chem. Phys. Lett.* **2009**, *471* (1−3), 1−10.

(3) Kreisel, K. A.; Yap, G. P. A.; Dmitrenko, O.; Landis, C. R.; Theopold, K. H. *J. Am. Chem. Soc.* **2007**, *129*, 14162−16163.
(4) Tsai, Y. C.; Hsu, C. W.; Yu, J. S. K.; Lee, G. H.; Wang, Y.; Kuo, T. S. *Angew. Chem., Int. Ed.* **2008**, *47*, 7250−7253.
(5) Hsu, C. W.; Yu, J. S. K.; Yen, C. H.; Lee, G. H.; Wang, Y.; Tsai, Y. C. *Angew. Chem., Int. Ed.* **2008**, *47*, 9933−9936.
(6) Wagner, F. R.; Noor, A.; Kempe, R. *Nat. Chem.* **2009**, *1*, 529−536.
(7) Wu, L.-C.; Hsu, C.-W.; Chuang, Y.-C.; Lee, G.-H.; Tsai, Y.-C.; Wang, Y. *J. Phys. Chem. A* **2011**, *115* (45), 12602−12615.
(8) La Macchia, G.; Veryazov, V.; Roos, B. O.; Gagliardi, L. *Inorg. Chem.* **2008**, *47* (24), 11455−11457.
(9) Ziegler, T.; Rauk, A. *Theor. Chim. Acta* **1977**, *46*, 1.
(10) Michalak, A.; Mitoraj, M.; Ziegler, T. *J. Phys. Chem. A* **2008**, *112*, 1933.
(11) Mitoraj, M.; Michalak, A.; Ziegler, T. *J. Chem. Theory Comput.* **2009**, *5*, 962−975.
(12) Ziegler, T.; Rauk, A. *Inorg. Chem.* **1979**, *18*, 1755.
(13) Ziegler, T.; Rauk, A. *Inorg. Chem.* **1979**, *18*, 1558.
(14) Nalewajski, R. F.; Mrozek, J. *Int. J. Quantum Chem.* **1996**, *57*, 377−389.
(15) Michalak, A.; De Kock, R.; Ziegler, T. *J. Phys. Chem. A* **2008**, *112*, 7256−7263.
(16) Schwarz, W. H. E.; Schmidbaur, H. *Chem.—Eur. J.* **2012**, *18*, 4470−4479.
(17) Grimme, S.; Ehrlich, S.; Goerigk, L. J. *Comput. Chem* **2011**, *32*, 1456.
(18) Te Velde, G.; Bickelhaupt, F. M.; Baerends, E. J.; van Gisbergen, S. J. A; Guerra, C.; Snijders, J. G.; Ziegler, T. *J. Comput. Chem.* **2001**, *22*, 931.
(19) Becke, A. *Phys. Rev. B* **1988**, *38*, 3098−3100.
(20) Perdew, J. *Phys. Rev. B* **1986**, *33*, 8822−8824.
(21) Gabriel, M.; Kelling, J. D.; Jason, S. D.; Roald, H. *J. Am. Chem. Soc.* **2007**, *129* (49), 15295−15302.
(22) Frenking, G. *Science* **2005**, *310* (5749), 796−797.
(23) Clark, R. L.; Frank, W. *J. Am. Chem. Soc.* **2006**, *128* (22), 7335−7345.
(24) Awal, N.; Rhett, K. *Chem. Rec.* **2010**, *10*, 413−416.
(25) Wolf, R.; Ni, C.; Nguyen, T.; Brynda, M.; Long, G. J.; Sutton, A. D.; Fischer, R. C.; Fettinger, J. C.; Hellman, M.; Pu, L.; Power, P. P. *Inorg. Chem.* **2007**, *46*, 11277.